Macromolecules

ARTICLE

pubs.acs.org/Macromolecules

Effect of Nanoscale Morphology on the Conductivity of Polymerized Ionic Liquid Block Copolymers

Ryan L. Weber,[†] Yuesheng Ye,[‡] Andrew L. Schmitt,[†] Steven M. Banik,[†] Yossef A. Elabd,[‡,*] and Mahesh K. Mahanthappa[†,*]

[†]Department of Chemistry, University of Wisconsin—Madison, 1101 University Avenue, Madison, Wisconsin 53706, United States

[‡]Department of Chemical and Biological Engineering, Drexel University, Philadelphia, Pennsylvania 19104, United States

Supporting Information

ABSTRACT: Polymerized ionic liquid (POIL) block copolymers represent a unique class of materials for fundamental studies of single ion conduction as a function of morphology in microphase-separated polymer electrolytes for energy storage and conversion applications. We describe the synthesis of a series of poly(styrene-*b*-4-vinylbenzyl-alkylimidazolium bis(trifluoromethanesulfonyl)imide) (PS-*b*-PVBn-(alkyl)ImTFSI; alkyl = CH_3 (Me), *n*-C_4H_9 (Bu), *n*-C_6H_{13} (Hex)) diblock copolymers (2.7−17.0 mol % POIL) via exhaustive functionalization and ion exchange of relatively narrow molecular weight dispersity poly(styrene-*b*-4-vinylbenzyl chloride) precursors derived from nitroxide-mediated block copolymerizations. The solid-state morphology of these PS-*b*-PVBn(alkyl)ImTFSI copolymers were studied using a combination of temperature-dependent synchrotron small-angle X-ray scattering (SAXS) and transmission electron microscopy (TEM). From electrochemical impedance spectroscopy measurements, we observe that lamellar samples having similar compositions exhibit comparable values of conductivity (0.1 mS cm^{-1} at 150 °C) regardless of imidazolium alkyl substituent. The ionic conductivity of a compositionally varied series of PS-*b*-PVBnHexImTFSI diblocks depends nonlinearly on POIL composition (0.01 mS cm^{-1} for 8.6 mol % POIL and 0.1 mS cm^{-1} for 17.0 mol % POIL at 150 °C), thus highlighting the influence of morphology on the observed ionic conductivity of POIL block copolymers for the first time. By using different polymer processing strategies, we further demonstrate that the ionic conductivity of a single sample (8.6 mol % POIL) may vary by more than one order of magnitude depending on the long-range ordering of the microphase separated morphology. These studies indicate that macroscopic connectivity and morphological defects strongly affect the observed conductivity in these materials.

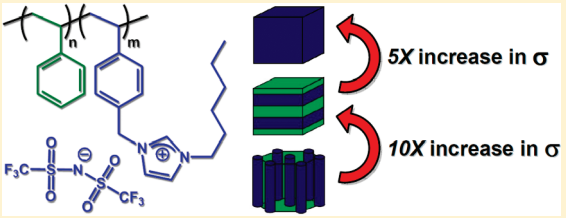

INTRODUCTION

As a consequence of their unique chemical and physical properties, polymerized ionic liquids (POILs) are emerging as a new class of materials with potential applications ranging from uses in catalysis,[1,2] nanomaterials synthesis,[3] gas separations media,[4−7] and as polymer electrolytes for battery and fuel cell applications.[8,9] A number of strategies have emerged for the application of ionic liquids in advanced materials applications, including the development of "ion gels" comprised of a polymer network swollen with an ionic liquid solvent.[10−12] A common problem encountered with both liquid electrolytes and ion gels is the propensity for electrolyte leakage from these systems. Polymerized ionic liquids enjoy many of the same favorable qualities as small molecule ionic liquids such as low flammability, chemical and thermal stability, and widely tunable physical properties, while mitigating concerns related to electrolyte leakage by virtue of their polymeric structures.[8] POIL "single-ion conductors" may thus serve as ideal polymer electrolytes for advanced electrical energy storage and conversion devices (e.g., fuel cells and batteries).

Recent studies of the ionic conductivity of polymerized ionic liquids have demonstrated that materials having low glass transition temperatures (T_g) are required to obtain high levels of ionic conductivity.[13−15] As a consequence of their low T_gs, these conductive materials are of limited use at ambient temperature in many electrochemical devices due to a lack of mechanical strength. While chemical cross-linking has been employed as a means to endow polymerized ionic liquids with greater mechanical strength,[16−21] block copolymers that self-assemble to form physically cross-linked, mechanically tough, nanostructured polymer electrolytes have attracted increased attention in the design of polymer electrolytes for electrochemical devices.[22] Microphase separated POIL-containing block copolymers provide an enticing opportunity to develop mechanically robust nanostructured materials, in which the ionic POIL domains form contiguous paths for ion conduction through a nonconducting matrix phase.

Despite numerous reports of microphase-separated ion conducting membranes, fundamental studies of the effect of nanoscale morphology on ionic conductivity are relatively scarce in anhydrous systems.[22] Balsara and co-workers studied lithium ion conduction in poly(styrene-*b*-ethylene oxide) block copolymers

Received: May 9, 2011
Revised: June 10, 2011
Published: June 24, 2011

exogenously doped with LiTFSI (TFSI = bis(trifluoromethanesulfonyl)imide) in the vicinity of order−order and order−disorder transitions.[23] The absence of discontinuities in conductivity across phase boundaries prompted them to conclude that morphology had little or no effect on conductivity, in the case when ion conducting blocks comprised the majority phase in the self-assembled morphology ($\varphi_{ionic} \geq 0.50$). Simone and Lodge studied poly(styrene-*b*-ethylene oxide) diblock copolymers swollen with ionic liquid and found that conductivity increased with increasing ionic liquid content and determined that morphologies having continuous ionic domains were significantly more conductive than those in which grain boundaries inhibit ion mobility.[24] Similarly, Elabd and co-workers investigated ionic conductivities of poly(styrene-*b*-methyl methacrylate) block copolymers containing up to 50 wt % ionic liquid and found higher values of conductivity with increasing connectivity among conducting domains.[25] While these studies provide important insights into the conductivity behavior of microphase separated ion conducting membranes, they all involve exogenous electrolytes doped into nonconducting block copolymers. To the best of our knowledge, no fundamental studies of the effect of morphology on ionic conductivity for anhydrous microphase separated POIL block copolymers exist in the literature. Such studies will be beneficial to the design of future polymeric single-ion conductors for energy storage and conversion devices.

Recent studies have demonstrated that the ionic conductivity characteristics of POIL homopolymers vary widely as a function of polymer structure and counterion and may be tailored for potential applications as fuel cell and battery polymer electrolytes. An underlying theme that emerges from the works reported by the groups of Colby,[26] Ohno,[13,27] and Elabd[14,15] is that the ionic conductivity of these polymers depends primarily on the glass transition temperatures (T_g) of these materials, reflecting the coupling of ion motion to polymer segmental dynamics. Recently, we described the modular synthesis and physical characterization of a new series of styrenic imidazolium-based polymerized ionic liquid homopolymers prepared by exhaustive functionalization of relatively narrow dispersity poly(4-vinylbenzyl chloride) with homologous *N*-alkylimidazoles.[28] In that study, we investigated the thermal properties and ionic conductivity of POILs having various counterions and imidazolium moieties at constant average polymer chain length, finding that POILs bearing *N*-hexylimidazolium groups and bis(trifluoromethanesulfonyl)imide (TFSI) counterions exhibited the highest nonhumidified ion conductivity (0.35 mS cm^{-1} at 150 °C).

In the present study, we prepared a series of poly(styrene-*b*-4-vinylbenzyl alkylimidazolium bis(trifluoromethanesulfonyl)imide) (PS-*b*-PVBn(alkyl)ImTFSI) block copolymers derived from post-synthetic modification of relatively narrow dispersity poly(styrene-*b*-4-vinylbenzyl chloride) produced by nitroxide-mediated polymerization (NMP). Films of the POIL diblock copolymers containing a rigid polystyrene block and a low-T_g POIL block were prepared via solvent-casting and melt-pressing with subsequent evaluation of their nanoscale morphology by temperature-dependent synchrotron small-angle X-ray scattering (SAXS) and transmission electron microscopy (TEM). Effects of morphology on the ionic conductivity of these single-ion conductors were investigated using electrochemical impedance spectroscopy (EIS). These effects were exemplified by an increase in ionic conductivity of more than an order of magnitude between a lamellar + cylindrical phase coexistence sample (8.6 mol % POIL) and a lamellar sample (17.0 mol % POIL), indicating the importance of connectivity among conductive domains. Additionally, a single sample exhibiting lamellar + cylindrical coexistence morphology (8.6 mol % POIL) showed a large disparity in conductivity depending on the degree of long-range order (solvent-cast *vs* melt-pressed samples).

EXPERIMENTAL SECTION

Materials. All chemicals were purchased from Sigma-Aldrich Chemical Co. (Milwaukee, WI) and were used as received unless otherwise noted. Copper(I) bromide was purified according to the literature.[29] Styrene was stirred over CaH_2 to remove inhibitors and then distilled under reduced pressure. 4-Vinylbenzyl chloride was purified by passage through silica gel using hexanes as an eluent followed by removal of hexanes *in vacuo*. *N*-Methylimidazole, *N*-butylimidazole, and *N*,*N*,*N*′,*N*″,*N*″-pentamethyldiethylenetriamine were distilled under reduced pressure. *N*-Hexylimidazole was synthesized by a slight modification of a literature procedure in which ethanol was used as a solvent instead of 1-propanol.[30] 2,2,5-Trimethyl-4-phenyl-3-azahexane 3-nitroxide (TIPNO) was prepared according to a previously reported literature procedure.[31]

^{1}H NMR spectra were recorded on Varian Inova 500, Varian Mercury Plus, or Bruker AC+ 300 spectrometers and were referenced relative to tetramethylsilane (in acetone-d_6 and $CDCl_3$) or the residual protiated solvent peak (in DMSO-d_6) in the samples. Block copolymer compositions were calculated using quantitative ^{1}H NMR spectroscopy, and M_n values for these samples were calculated using the M_n of the initial poly(styrene) macroinitiator determined from size exclusion chromatography.

Size Exclusion Chromatography (SEC). Molecular weights of the poly(styrene) macroinitiator and all molecular weight distributions were determined by SEC using a Visctoek GPCMax system using refractive index (RI) detection. Separations employed two Polymer Laboratories (Amherst, MA) Resipore columns (250 mm ×4.6 mm) using a THF eluent at 40 °C at a flow rate of 1.0 mL/min. The molecular weight of the poly(styrene) macroinitiator, as well as all reported polydispersity indices (M_w/M_n) are derived from a conventional poly(styrene) calibration curve constructed using 10 narrow molecular weight distribution standards having M_n = 580−377400 g/mol (Polymer Laboratories, Amherst, MA).

Differential Scanning Calorimetry. Glass transition temperatures (T_gs) were measured using a TA Instruments Q100 modulated differential scanning calorimeter under N_2 environment. The thermal history of samples hermetically sealed in aluminum pans was erased by heating to 150 °C for 3 min and cooling to −50 °C. Second heating curves recorded over a temperature range of −50 to +150 °C using a heating ramp rate of 5 °C/min were used to determine T_g by the midpoint method.

Small Angle X-ray Scattering. Synchrotron small-angle X-ray scattering (SAXS) measurements were performed at the 5-ID-D beamline of the DuPont-Northwestern-Dow Collaborative Access Team Synchrotron Research Center at the Advanced Photon Source (Argonne, IL). Experiments employed a beam energy of 16 keV (λ = 0.7293 Å) and a 3.068 m sample-to-detector distance. Two-dimensional SAXS patterns were recorded on a MAR-CCD detector (133 mm diameter active circular area) with 1024 × 1024 pixel resolution. Film samples were sandwiched between Kapton tape and placed in an array stage. Other samples were heated to the desired temperature in a Linkam DSC and allowed to equilibrate for 5 min before data collection (typical exposure times 0.1−1 s). 2D patterns were azimuthally integrated to obtain intensity *vs q* plots using DataSqueeze software package. In anisotropic 2D patterns, azimuthal integrations were performed along the long axis of the profiles to optimize the appearance of scattering reflections for definitive morphological assignment.

Transmission Electron Microscopy (TEM). Samples were sectioned using a RMC MT-7000 ultramicrotome at room temperature

using a diamond knife to produce section samples at 75−90 nm thickness. Specimens were placed on 400-mesh Cu grids and exposed to the vapor above a 5 wt % aqueous RuO_4 solution for 1.5 h to preferentially stain the poly(styrene) block. PS-*b*-PVBnHexImTFSI-7.1 was imaged without staining due to the natural contrast stemming from the higher $Z = 32$ sulfur atoms in the TFSI counterion. TEM micrographs were taken on an LEO EM 912 TEM operating at 120 kV.

Electrochemical Impedance Spectroscopy. The ionic conductivities of the polymerized ionic liquid (POIL) diblock copolymers were measured using electrochemical impedance spectroscopy (EIS) (Solartron, 1260 impedance analyzer, 1287 electrochemical interface, Zplot software) over a frequency range of 1 Hz to 10^6 Hz at 200 mV. The in-plane ionic conductivity was measured with a four-electrode method using a custom-made Teflon-coated stainless steel cell at controlled temperatures and a dry condition (10% relative humidity) in an environmental chamber (Tenney, BTRS model). An alternating current was applied to the outer electrodes and the real impedance or resistance, R, was measured between the two inner reference electrodes. The resistance was determined from a semicircle regression of the Nyquist data (imaginary *vs* real impedance), where the real impedance was taken as the x-intercept of this regression. Conductivity was calculated by using the following equation: $\sigma = L/AR$, where L and A are the distance between two inner electrodes and the cross-sectional area of the polymer film ($A = Wl$; W is the film width and l is the film thickness), respectively. The thicknesses of the polymer films (typically $\geq 100\ \mu$m) were measured with a Mitutoyo digital micrometer (± 0.001 mm). Samples were allowed to equilibrate for 2 h at each measurement condition followed by at least six measurements at that condition; the reported value is an average of these steady-state measurements.

Synthesis of 2,2,5-Trimethyl-3-(2-oxyethyl isobutryl)-4-phenyl-3-azahexane (1). Copper(I) bromide (0.12 g, 0.85 mmol) and copper(0) powder (3.24 g, 51.1 mmol) were placed in a 100 mL Schlenk flask under nitrogen. Ethyl α-bromoisobutyrate (3.37 g, 17.0 mmol), TIPNO (2.50 g, 11.3 mmol), *N*,*N*,*N*′,*N*″,*N*″-pentamethyldiethylenetriamine (0.14 g, 0.85 mmol), and *N*,*N*-dimethylformamide (40 mL) were combined in a second dry 100 mL Schlenk tube and freeze−thaw degassed four times. Under a flush of nitrogen, the latter solution was cannula transferred onto the copper mixture to yield a dark green solution. This reaction mixture was vigorously stirred at 40 °C for 60 min, during which time it turned dark blue, and then it was stirred overnight at 22 °C. The solution was subsequently filtered through a plug of neutral alumina, which was washed with ethyl acetate (250 mL). The combined organic eluents were concentrated on a rotary evaporator at 40 °C. The resulting crude product was purified by silica gel column chromatography (10 cm × 5 cm diameter) using hexanes/ethyl acetate (30:1 v/v) to furnish the alkoxyamine **1** as a yellow/orange viscous liquid. Yield: 3.41 g (90% yield). ^{1}H NMR (300 MHz, $CDCl_3$, 22 °C): δ (ppm) 7.63−7.16 (m, 5 H, −Ar−*H*, both diastereomers), 4.28−4.06 (m, 2H, O−CH_2−CH_3, both diastereomers), 3.70 (d, $J_{H-H}{}^3$ = 10.8 Hz, 1H, N−C*H*, minor diastereomer), 3.42 (d, $J_{H-H}{}^3$ = 10.8 Hz, 1H, N−C*H*, major diastereomer), 2.48−2.34 (m, 1H, C*H*$(CH_3)_2$, minor diastereomer), 1.90−1.76 (m, 1H, C*H*$(CH_3)_2$, major diastereomer), 1.62 (s, 3H, C$(CH_3)_2$, major diastereomer, rotamer A), 1.59 (s, 3H, C$(CH_3)_2$, minor diastereomer, rotamer A), 1.55 (s, 3H, C$(CH_3)_2$, major diastereomer, rotamer B), 1.48 (s, 3H, C$(CH_3)_2$, minor diastereomer, rotamer B), 1.31 (t, $J_{H-H}{}^3$ = 7.2 Hz, 3H, O−CH_2−CH_3, minor diastereomer), 1.28 (t, $J_{H-H}{}^3$ = 7.2 Hz, 3H, O−CH_2−CH_3, major diastereomer), 1.24 (d, $J_{H-H}{}^3$ = 6.2 Hz, 3H, CH$(CH_3)_2$, minor diastereomer, rotamer A), 1.16 (d, $J_{H-H}{}^3$ = 6.2 Hz, 3H, CH$(CH_3)_2$, major diastereomer, rotamer A), 0.93 (s, 9H, C$(CH_3)_3$, major diastereomer), 0.81 (s, 9H, C$(CH_3)_3$, minor diastereomer), 0.72 (d, $J_{H-H}{}^3$ = 6.8 Hz, 3H, CH$(CH_3)_2$, minor diastereomer, rotamer B), 0.39 (d, $J_{H-H}{}^3$ = 6.8 Hz, 3H, CH$(CH_3)_2$, major diastereomer, rotamer B). The ^{1}H NMR spectrum is provided in the Supporting Information (Figure S1). ^{13}C NMR (75 MHz, $CDCl_3$, 22 °C): δ (ppm, all stereoisomers and rotamers) 175.26, 175.03, 142.04, 140.62, 131.01, 130.26, 127.35, 127.11, 126.50, 126.10, 81.86, 79.57, 73.74, 72.42, 60.57, 60.32, 30.75, 30.18, 28.23, 27.29, 25.97, 25.23, 24.59, 22.83, 22.66, 22.55, 22.06, 21.88, 20.97, 13.94. ESI−MS: calcd. for $C_{20}H_{33}NO_3$ $[M + Na]^+$, 358.2; found, 358.3.

Synthesis of Polystyrene Macroinitiator (PS-TIPNO). Freshly purified styrene (34.9 g, 336 mmol) and alkoxyamine **1** (0.322 g, 0.96 mmol) were sealed in a 100 mL Schlenk flask and subjected to four freeze−thaw degassing cycles, after which the flask contents were placed under N_2(g). The flask was placed in an oil bath thermostated at 125 °C and stirred for 6 h 10 min, after which it was chilled in dry ice/isopropanol for 10 min before exposure to air. The polymerization reaction was diluted with dichloromethane (60 mL) and twice precipitated into methanol (2 L). Yield: 20.3 g of white powder (58% conversion). ^{1}H NMR (300 MHz, $CDCl_3$, 22 °C): δ (ppm) 7.30−6.86 (m, 3 H, Ar−*H meta* + *para*), 6.85−6.27 (m, 2 H, Ar−*H ortho*), 2.30−1.66 (m, 1 H, CH_2C*H*), 1.66−1.07 (m, 2 H, CH_2CH). SEC (THF, 40 °C): M_n = 19.1 kg/mol, M_w/M_n = 1.14 (against PS standards).

Representative Synthesis of Poly(styrene-*b*-4-vinylbenzyl chloride) (PS-*b*-PVBCl). Freshly purified 4-(vinylbenzyl choride) (2.39 g, 15.7 mmol), PS-TIPNO (3.0 g, 0.157 mmol), and xylenes (9.05 mL) were freeze−thaw degassed (4x) in a 50 mL Schlenk tube, after which the flask contents were left under vacuum. The flask was placed in an oil bath thermostated at 110 °C and stirred for a designated amount of time, after which it was chilled in dry ice/isopropanol for 10 min before exposure to air. The polymerization reaction was diluted with dichloromethane (10 mL) and twice precipitated into methanol (500 mL). Yield: 3.71 g of white powder (30% conversion). $M_{n,NMR}$ = 25.1 kg/mol (17.6 mol % VBCl composition from quantitative ^{1}H NMR) M_w/M_n = 1.26 (against PS standards). ^{1}H NMR (300 MHz, $CDCl_3$, 22 °C): δ (ppm) 7.43−6.85 (m, 16.0 H, Ar−*H meta* + *para*), 6.85−6.13 (m, 11.4 H, Ar−*H ortho*), 4.64−4.30 (2.0 H, CH_2Cl), 2.42−1.06 (m, 17.5 H, CH_2C*H*).

Representative Synthesis of PS-*b*-PVBnHexImCl. Poly(styrene-*b*-4-vinylbenzyl chloride) (3.0 g, 0.134 mmol, DP_{VBC} = 21.6) and *N*-hexylimidazole (3.2 g, 21.3 mmol) were dissolved in $CHCl_3$ (10.2 mL) and heated to 55 °C for 24 h. The reaction mixture was then diluted with $CHCl_3$ (10 mL), and the polymer was twice precipitated into rapidly stirred hexanes (500 mL) before vacuum drying. ^{1}H NMR analysis still showed traces of *N*-hexylimidazole, however, this material was pure enough for subsequent reactions. Yield: 3.21 g of white powder (93% yield). ^{1}H NMR (300 MHz, DMSO-d_6, 22 °C): δ (ppm) 10.63−9.88 (1.0 H, N═C*H*N), 8.43−5.09 (m, 32.1 H, NC*H*═C*H*N, Ar−*H*, and ArCH_2N), 4.17 (s, 2.0 H, NC$H_2C_5H_{11}$), 2.23−0.49 (m, 26.6 H, CH_2C*H* and $CH_2C_5H_{11}$).

Synthesis of PS-*b*-PVBnMeImCl. Poly(styrene-*b*-4-vinylbenzyl chloride) (0.75 g, 0.030 mmol, DP_{VBC} = 39.5) and *N*-methylimidazole (1.18 g, 14.4 mmol) were dissolved in *N*,*N*-dimethylformamide (DMF) (4.0 mL) and heated to 80 °C for 16 h, during which time the solution became cloudy and yellow in color. DMF was removed under vacuum at 50 °C and the residue was triturated with deionized water (15 mL) for 2 h before isolation by centrifugation, decanting the cloudy supernatant liquid, and vacuum drying at 50 °C. ^{1}H NMR analysis still showed traces of *N*-methylimidazole, however, this material was pure enough for subsequent reactions. Yield: 0.76 g of off-white powder (90% yield). ^{1}H NMR (300 MHz, DMSO-d_6, 22 °C): δ (ppm) 10.31−9.73 (m, 1.0 H, N═C*H*N), 8.28−5.12 (m, 19.7 H, NC*H*═C*H*N, Ar−*H* and ArCH_2N), 3.87 (s, 3.0 H, NCH_3), 2.24−0.74 (6.7 H, CH_2C*H*).

Synthesis of PS-*b*-PVBnBuImCl. The synthesis of PS-*b*-PVBnBuImCl follows that of PS-*b*-PVBnMeImCl. Yield: 0.87 g of off-white powder (96% yield). ^{1}H NMR (300 MHz, DMSO-d_6, 22 °C): δ (ppm) 10.72−9.97 (m, 1.0 H, N═C*H*N), 8.73−5.08 (m, 23.8 H, NC*H*═C*H*N, Ar−*H* and ArCH_2N), 4.20 (s, 2.0 H, NC$H_2C_3H_7$), 2.24−0.22 (m, 17.7 H, CH_2C*H* and $CH_2C_3H_7$).

Representative Synthesis of PS-*b*-PVBnHexImTFSI. PS-*b*-PVBnHexImCl (0.64 g, 0.021 mmol, $DP_{VBnHexImCl}$ = 39.2), lithium bis(trifluoromethanesulfonyl)imide (0.72 g, 2.5 mmol), and tetrahydrofuran (THF) (4 mL) were stirred at 55 °C for 24 h, then at 22 °C for 24 h. The reaction mixture was concentrated to a viscous solution and precipitated by adding methanol/water (1:1 v/v) dropwise to the polymer solution. After stirring several minutes, the slurry was centrifuged and the supernatant liquid was decanted before vacuum drying at 50 °C. The polymer was redissolved in a minimum amount of THF and then precipitated twice more by the same procedure until combustion of a small polymer sample no longer resulted in the observation of a red colored flame indicative of the presence of lithium.[32] Finally, the polymer was triturated with pentanes (10 mL) for several hours before vacuum drying at 60 °C. Yield: 0.78 g of white powder (93% yield). ^{1}H NMR (500 MHz, acetone-d_6, 22 °C): δ (ppm) 9.04 (s, 1.0 H, N=C*H*N), 7.90−6.90 (m, 20.4 H, NC*H*=C*H*N and Ar−*H meta* + *para*), 6.88−6.33 (m, 11.8 H, Ar−*H ortho*), 5.63−5.18 (m, 2.0 H, ArCH_2N), 4.32 (s, 2.0 H, N$CH_2C_5H_{11}$), 2.51−1.19 (m, 26.5 H, CH_2CH and $CH_2-C_4H_8-CH_3$), 0.85 (s, 3.0 H, CH_3). Anal. Calcd: C, 67.04; H, 6.10; N, 3.97; F, 10.77; Cl, 0.00. Found: C, 65.80; H, 5.93; N, 4.16; F, 10.90; Cl, 0.0.

Synthesis of PS-*b*-PVBnMeImTFSI. The synthesis of PS-*b*-PVBnMeImTFSI follows that of PS-*b*-PVBnHexImTFSI, except that *N*,*N*-dimethylformamide was used as the reaction solvent. Yield: 0.81 g of white powder (80% yield). ^{1}H NMR (500 MHz, acetone-d_6, 22 °C): δ (ppm) 8.93 (s, 1H, N=C*H*N), 7.78−6.90 (m, 21.8 H, NC*H*=C*H*N and Ar−*H meta* + *para*), 6.88−6.33 (m, 12.8 H, Ar−*H ortho*), 5.57−5.25 (m, 2.0 H, ArCH_2N), 3.99 (s, 2.0 H, NCH_3), 2.52−1.20 (m, 19.8 H, CH_2CH). Anal. Calcd: C, 67.12; H, 5.63; N, 4.03; F, 10.93; Cl, 0.00. Found: C, 66.86; H, 5.56; N, 3.88; F, 10.65; Cl, <0.25.

Synthesis of PS-*b*-PVBnBuImTFSI. The synthesis of PS-*b*-PVBnBuImTFSI follows that of PS-*b*-PVBnHexImTFSI, except that *N*,*N*-dimethylformamide was used as the reaction solvent. Yield: 1.03 g of white powder (87% yield). ^{1}H NMR (500 MHz, acetone-d_6, 22 °C): δ (ppm) 9.02 (s, 1.0 H, N=C*H*N), 7.86−6.90 (m, 20.0 H, NC*H*=C*H*N and Ar−*H meta* + *para*), 6.88−6.30 (m, 12.0 H, Ar−*H ortho*), 5.59−5.23 (m, 2.0 H, ArCH_2N), 4.31 (s, 2.0 H, N$CH_2C_3H_7$), 2.51−1.19 (m, 21.5 H, CH_2CH and $CH_2-C_2H_4-CH_3$), 0.91 (s, 3.0 H, CH_3). Anal. Calcd: C, 66.81; H, 5.90; N, 4.04; F, 10.95; Cl, 0.00. Found: C, 66.76; H, 5.82; N, 3.95; F, 10.79; Cl, 0.0.

Solvent-Casting PS-*b*-PVBn(alkyl)ImTFSI Block Copolymers. Polymer solutions (7% w/w) in dry THF were prepared in vials. Glass substrates (approximately 4 mm ×45 mm) were cut from microscope slides and cleaned with acetone. Substrates were placed in the bottom of a Petri dish and then polymer solutions were cast on top of the substrates via pipet. The cover was placed on top of the Petri dish and the solvent was allowed to evaporate for 1−2 h before another layer of polymer solution was cast on top of the films. This process was repeated one more time for especially brittle samples. The films were allowed to air-dry inside the Petri dish overnight at ambient temperature. Polymer films were vacuum annealed at 150 °C for 3 h before slowly cooling to ambient temperature under vacuum.

Melt-Pressing PS-*b*-PVBnHexImTFSI Block Copolymers. As a comparison to solvent-cast films, polymer films were also prepared by melt pressing. The polymer in powder form was melt-pressed (Carver, Model 3851-0) at 150 °C, 3500 psi for 10 min into a film of 190 μm in thickness. The melt-pressed films were then annealed at 150 °C under vacuum for 3 days and then stored in a desiccator until further use.

RESULTS AND DISCUSSION

Block Copolymer Synthesis. We synthesized a series of POIL block copolymers by exhaustive functionalization of poly(styrene-*b*-4-vinylbenzyl chloride) (PS-*b*-PVBCl) diblock copolymers synthesized by nitroxide mediated polymerization (NMP) as previously reported by Stancik et al.[33] A single batch of relatively narrow dispersity polystyrene macroinitiator with M_n = 19.1 kg/mol was synthesized using alkoxyamine **1** with a high level of control (M_w/M_n = 1.14). We subsequently produced a series of poly(styrene-*b*-4-vinylbenzyl chloride) (PS-*b*-PVBCl) diblock copolymers via chain extension of the polystyrene macroinitiator (Scheme 1). Initial attempts to grow diblock copolymers at 125 °C resulted in broad and bimodal molecular weight distributions due to the fast rate of propagation of the VBCl monomer relative to the initiation of the polystyryl chain ends. Efforts to slow propagation by addition of excess TIPNO free radical (50−100 mol % with respect to macroinitiator) resulted in bimodal distributions. Thus, we were able to dramatically decrease the rate of polymerization and increase the overall degree of control by lowering the apparent polymerization temperature from 125 to 110 °C and by running the polymerizations under static vacuum. We obtained four PS-*b*-PVBCl diblock copolymers with unimodal molecular weight distributions ranging from M_w/M_n = 1.20−1.26 depending on the VBCl incorporation as outlined in Table 1. Representative size exclusion chromatography (SEC) traces of the polystyrene macroinitiator and PS-*b*-PVBCl-17.6 block copolymer are shown in Figure 1.

Exhaustive functionalization of the PS-*b*-PVBCl block copolymers with excess *N*-alkylimidazole in either $CHCl_3$ at 55 °C or DMF at 80 °C over 24 h quantitatively yielded PS-*b*-PVBn(alkyl)ImCl diblock copolymers (alkyl = CH_3 (Me), *n*-C_4H_9 (Bu), or *n*-C_6H_{13} (Hex)) (Scheme 2). In order to accurately probe the effects of nanoscale morphology on ionic conductivity,

Scheme 1. Synthesis of Poly(styrene-*b*-4-vinylbenzyl chloride) (PS-*b*-PVBCl) Block Copolymers

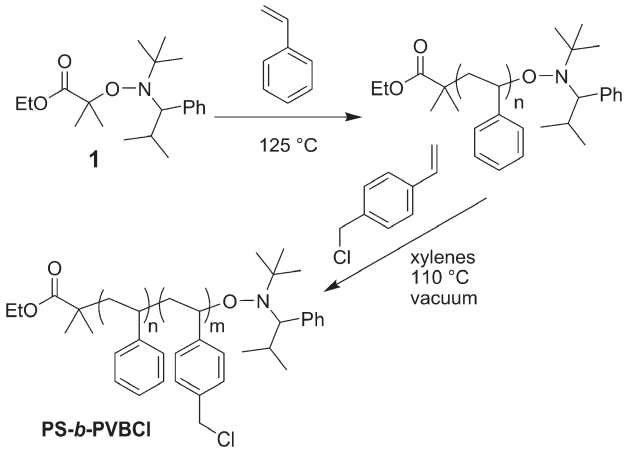

Table 1. Molecular Parameters of PS-*b*-PVBCl Diblock Copolymer Precursors to POIL-Containing Block Copolymers

polymer	VBCl mol %[a]	$M_{n(tot)}$ (kg/mol)[a]	M_w/M_n[b]
PS-*b*-PVBCl-4.8	4.8	20.5	1.20
PS-*b*-PVBCl-8.3	8.3	21.7	1.21
PS-*b*-PVBCl-10.5	10.5	22.4	1.23
PS-*b*-PVBCl-17.6	17.6	25.1	1.26

[a] Determined by quantitative ^{1}H NMR and the M_n = 19.1 kg/mol for the initial PS-TIPNO macroinitiator. [b] Determined by SEC using conventional calibration with PS standards.

Scheme 2. Synthesis of Poly(styrene-*b*-4-vinylbenzyl alkylimidazolium TFSI) Block Copolymers

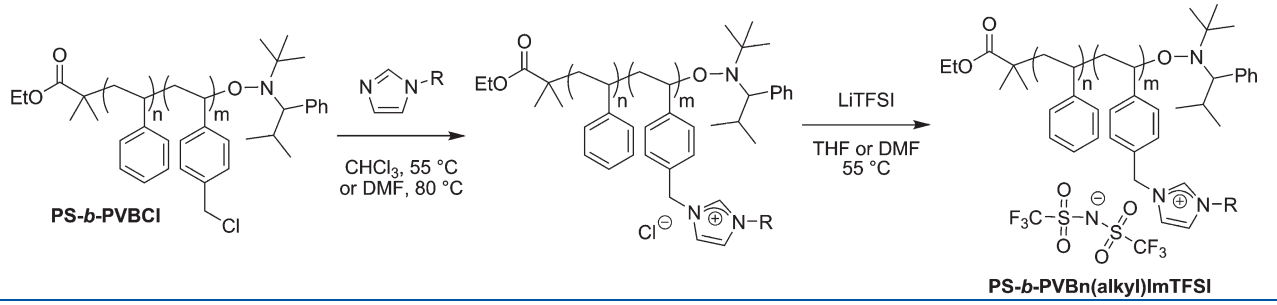

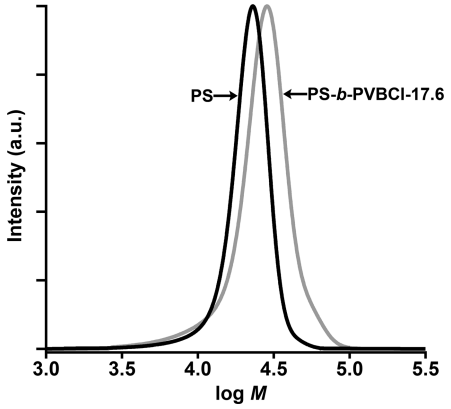

Figure 1. Representative SEC refractive index traces of polystyrene macroinitiator and PS-*b*-PVBCl-17.6 diblock copolymer.

we sought to study a POIL system with a relatively high intrinsic conductivity that does not sensitively depend on external variables such as humidification. Following recent reports indicating that hydrophobic methacrylate-based POILs bearing bis(trifluoromethanesulfonyl)imide (TFSI) counterions exhibit high ionic conductivities due to their low glass transition temperatures, we exchanged all counterions in our diblock copolymers for TFSI.[14] Therefore, exhaustive salt methatheses of the PS-*b*-PVBn(alkyl)-ImCl having varying POIL contents with LiTFSI furnished a series of PS-*b*-PVBn(alkyl)ImTFSI diblock copolymers. Differential scanning calorimetry (DSC) showed that all of the polymers exhibited low glass transition temperatures $T_g \sim 9$ °C for the POIL blocks regardless of alkyl substituent. High field ^{1}H NMR of the resulting block copolymers in acetone-d_6 revealed that the polymer compositions deviated slightly from those of their PS-*b*-PVBCl precursors, likely due to fractionation during polymer isolation. Figure 2 shows representative ^{1}H NMR spectra of PS-*b*-PVBnHexImTFSI and the corresponding PS-*b*-PVBCl precursor. In each case, polymer compositions were determined by relative integrations of the indicated ^{1}H resonances.

Morphological Characterization. The self-assembly behavior of PS-*b*-POIL block copolymers was investigated using synchrotron small-angle X-ray scattering (SAXS) at room temperature. Initial SAXS studies of powder and melt-pressed samples demonstrated a low degree of long-range order in POIL block copolymers evidenced by broad and poorly defined higher order scattering maxima, likely a result of the strong segregation between the ionic and hydrophobic blocks that frustrates ordering. In an effort to effect higher degrees of long-range nanoscale order in these samples, we solvent-cast films from THF onto glass substrates and vacuum annealed them for 3 h at 150 °C. In order

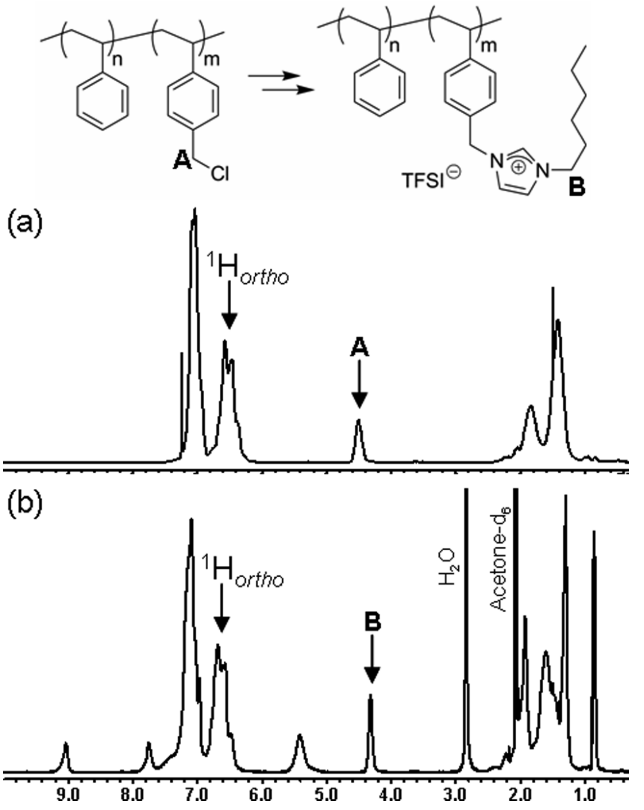

Figure 2. ^{1}H NMR spectra of (a) PS-*b*-PVBCl-17.6 in $CDCl_3$ and (b) PS-*b*-PVBnHexImTFSI-17.0 in acetone-d_6. Diblock compositions are calculated from relative integrations of resonances A or B versus the sum of all styrenic *ortho* proton resonances.

to assess bulk morphologies of these samples using variable temperature SAXS, sacrificial samples of these solvent-cast films were ground into powders. Solvent-cast films used for conductivity studies (*vide infra*) were carefully removed from the glass substrates using Kapton tape and subjected to SAXS analysis with the incident X-ray beam oriented normal to the film plane to assess morphology, level of order, and any possible preferential domain orientation (anisotropy). Samples that proved too brittle for effective solvent casting were melt-pressed into thin films. Because of the sensitivity of electrochemical impedance measurements of ionic conductivity to the alignment of microphase separated domains,[25,34] we analyzed the 2D scattering images of each film for any significant anisotropy. (Figure S2, Supporting Information). For solvent-cast samples, 2D scattering analysis shows little to no anisotropy in the alignment of domains, whereas

dx.doi.org/10.1021/ma201067h |*Macromolecules* 2011, 44, 5727–5735

for melt-pressed samples, a slight degree of anisotropy is observed due to flow experienced during the melt-pressing process. In such samples, we have disregarded this low level of anisotropy in our analyses of the conductivity data.

The morphologies of POIL block copolymer films were determined by indexing azimuthally integrated synchrotron SAXS profiles (Figure 3). Solvent-cast PS-*b*-PVBn(alkyl)ImTFSI block copolymers having 15−17% molar composition of the ionic polymer microphase separate into lamellae with a high degree of long-range order, regardless of the alkyl substituent (alkyl = CH_3, C_4H_9, or C_6H_{13}). For PS-*b*-PVBnMeImTFSI-15.6 and PS-*b*-PVBnBuImTFSI-16.7, the appearance of up to seven reflections at q^*, $2q^*$, $3q^*$, $4q^*$, $5q^*$, $6q^*$, and $7q^*$ clearly indicates a lamellar morphology. The profile of PS-*b*-PVBnHexImTFSI-17.0 exhibits reflections at q^*, $3q^*$, and $5q^*$, with structure factor extinctions of $2q^*$ and $4q^*$, indicative of a lamellar morphology with apparent

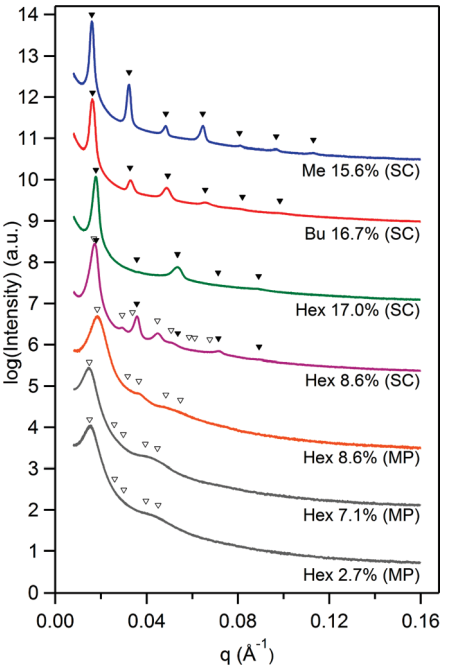

Figure 3. Azimuthally integrated SAXS profiles of PS-*b*-PVBn(alkyl)ImTFSI block copolymer films at 25 °C. Each trace is labeled by the imidazolium alkyl substitutent, POIL mole fraction, and processing method (SC = solvent cast; MP = melt-pressed). Solid and open arrows indicate reflections associated with lamellar (▼-LAM) and hexagonally packed cylinders (▽-CYL) morphologies, respectively.

symmetric volume fractions of each block.[35] Domain spacings for these lamellar samples range from 35 to 39 nm. POIL block copolymers were also subjected to variable-temperature SAXS to identify any order−order transitions or order−disorder transitions in the range 25−150 °C (Figure S3, Supporting Information). In all cases, we observed no order−order transitions or order−disorder transitions in this temperature range and only minor deviations in domain spacing.

Two complementary films of PS-*b*-PVBnHexImTFSI-8.6 prepared via solvent-casting and melt-pressing exemplify differences between these preparation techniques. The solvent-cast film exhibits coexistence between lamellar and hexagonally packed cylindrical morphologies sharing a single, slightly broadened primary scattering peak. Simone and Lodge saw similar coexistence phases in PS-*b*-PEO diblock copolymers preferentially swelled with ionic liquid where cylinders/lamellae coexistence was observed in place of gyroid morphology due to high segregation strength.[24] The lamellar morphology is evidenced by higher order reflections at $2q^*$, $4q^*$, and $5q^*$ with structure factor extinctions of $3q^*$ and $6q^*$ suggesting an apparent 33% volume composition of the ionic block.[35] The higher order reflections indicative of hexagonally packed cylindrical morphology are also seen at $q^*\sqrt{3}$, $2q^*$, $q^*\sqrt{7}$, and $3q^*$. Domain spacings of the cylinders and lamellae are 37 and 35 nm, respectively, which is roughly consistent with the expected epitaxial relationship between these two phases. An expansion of the azimuthally integrated SAXS pattern for this film is provided in the Supporting Information (Figure S4). Confirmation of phase coexistence is provided by transmission electron microscopy (TEM), in which both hexagonally packed cylinders and lamellar grains are observed (Figure 4a). In contrast, the SAXS profile of PS-*b*-PVBnHexImTFSI-8.6 prepared by melt-pressing exhibits broad features consistent with poorly ordered hexagonally packed cylinders morphology, although coexistence with lamellae cannot be ruled out due to the broad SAXS scattering maxima. A broad primary scattering peak is accompanied by a peak spanning $q^*\sqrt{3}$ and $2q^*$ and another shoulder spanning $q^*\sqrt{7}$ and $3q^*$. Similar to the solvent-cast sample, TEM studies show that this sample exhibits a coexistence of lamellar and cylindrical morphologies with a low degree of long-range order (Figure 4b). A difference in domain spacing (34 nm) relative to that seen for the solvent-cast sample (37 nm) is likely due to sample anisotropy induced by the melt-pressing process (Figure S2, Supporting Information).

Moving to lower POIL compositions, the SAXS profiles of melt-pressed PS-*b*-PVBnHexImTFSI-7.1 and PS-*b*-PVBnHexImTFSI-2.7 exhibit fewer features, making assignment of morphology more difficult. The similar profiles of these two films suggest

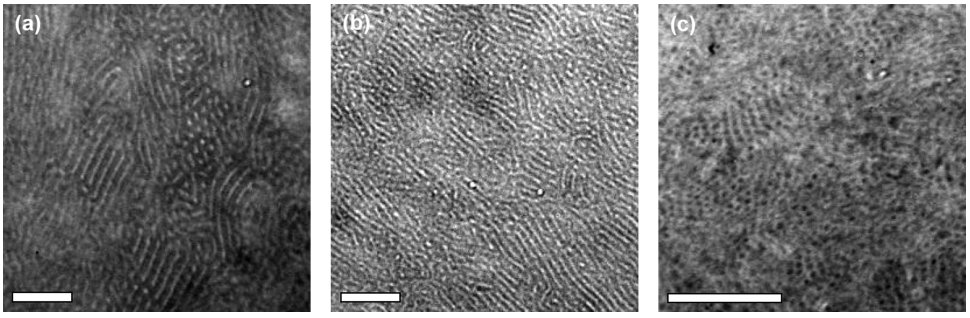

Figure 4. TEM images of (a) cylinders + lamellae phase coexistence exhibited by solvent-cast PS-*b*-PVBnHexImTFSI-8.6 in which the PS domains stained with RuO_4 appear dark, scale bar is 200 nm; (b) the cylinders + lamellae phase coexistence exhibited by melt-pressed PS-*b*-PVBnHexImTFSI-8.6 in which the PS domains stained with RuO_4 appear dark, scale bar is 200 nm; and (c) the hexagonally packed cylindrical morphology in melt-pressed PS-*b*-PVBnHexImTFSI-7.1 wherein the PVBnHexImTFSI domains appear dark due to the natural electron density contrast, scale bar is 500 nm.

Table 2. Molecular Properties and Morphologies of POIL Diblock Copolymers

diblock copolymer	M_n (kg/mol)[a]	POIL mol %[b]	φ_{POIL}[c]	morphology[d]	domain spacing (nm)[f]	POIL T_g (°C)[g]
PS-*b*-PVBnMeImTFSI-15.6	38.0	15.6	-	LAM	39	9
PS-*b*-PVBnBuImTFSI-16.7	39.6	16.7	-	LAM	38	9
PS-*b*-PVBnHexImTFSI-17.0	40.7	17.0	0.50	LAM	35	9
PS-*b*-PVBnHexImTFSI-8.6	31.0	8.6	0.34	LAM + CYL (SC)[e]	35/37	9
				LAM + CYL (MP)[e]	34	
PS-*b*-PVBnHexImTFSI-7.1	28.3	7.1	0.29	CYL	42	9
PS-*b*-PVBnHexImTFSI-2.7	24.2	2.7	0.19	CYL	42	9
PVBnHexImTFSI	57.5	100	1.00	-	n/a	9

[a] Calculated from PS-*b*-PVBCl M_n. [b] Determined by quantitative ^{1}H NMR of PS-*b*-POILs. [c] Volume fraction of POIL block determined using ρ(PS) = 0.969 g/cm^3 and ρ(PVBnHexImTFSI) = 1.096 g/cm^3 at 150 °C (see Supporting Information for details). [d] Determined by SAXS and TEM. [e] SC = solvent-cast; MP = melt-pressed. [f] Determined by SAXS using the position of the principal reflection. [g] Determined by DSC.

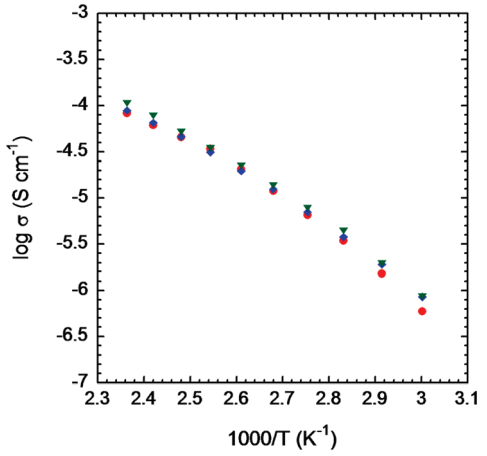

Figure 5. Effect of alkyl chain length on the temperature-dependent in-plane ionic conductivity of POIL diblock copolymers: PS-*b*-PVBnMeImTFSI-15.6 (red ●), PS-*b*-PVBnBuImTFSI-16.7 (blue ◆), PS-*b*-PVBnHexImTFSI-17.0 (green ▼).

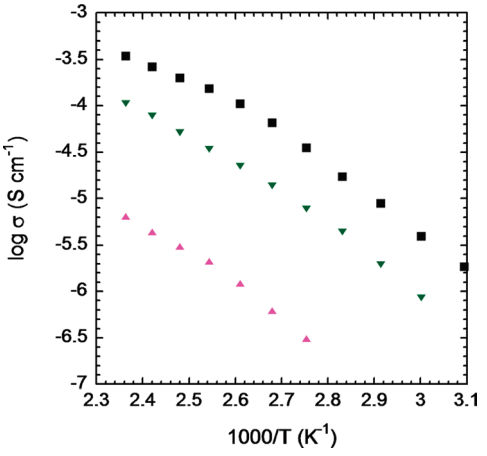

Figure 6. Effect of composition on the temperature-dependent in-plane ionic conductivity of POIL diblock copolymers: PVBnHexImTFSI (■), PS-*b*-PVBnHexImTFSI-17.0 (green ▼), and PS-*b*-PVBnHexImTFSI-8.6 (violet ▲).

poorly ordered hexagonally packed cylinders morphology as evidenced by broad primary scattering peaks with broad higher order peaks spanning $q^*\sqrt{7}$ and $3q^*$. The assignment of a hexagonally packed cylindrical morphology was confirmed with TEM (Figure 4c). A striking feature of these SAXS profiles is that the primary scattering peaks are significantly shifted to lower q, corresponding to an increased domain spacing (cylinder center-to-center distance) of 42 nm. We propose that this shift is due to swelling of the polystyrene domains by chains having little or no POIL incorporation, as a consequence of the synthetic route used to produce these materials. In the synthesis of the PS-*b*-PVBCl from which we derive our PS−POIL block copolymers, we polymerized the VBCl to relatively low monomer conversions. At such low monomer conversions, controlled living radical polymerizations initially yield materials with high polydispersities that only narrow as the polymerization progresses.[31] Thus, the high polydispersities of the PVBCl blocks of the PS−POIL precursors imply that there are a substantial number of chains that have few (if any) VBCl units, which translates into a substantial number of PS−POIL chains containing one or fewer POIL monomer units.[36] These POIL-deficient chains act as PS homopolymers that swell the polystyrene domains, thus giving rise to the observed increase in domain spacing for these samples.

The domain spacings for microphase separated POIL block copolymers (Table 2) suggest that a high degree of conformational asymmetry exists in the block copolymer melts consistent with a strongly segregated system in which the POIL segments exhibit high degrees of chain-stretching. The block copolymers exhibit domain spacings in the range of 34−42 nm, which is comparable to the calculated contour length of a fully extended chain (47−55 nm), suggesting that chains are highly stretched. Stancik et al. also observed high levels of chain stretching in PS−POIL block copolymers in neutron scattering studies of PS-*b*-PVBnMeImX (X = Cl, BF_4) that form elongated micelles.[33]

Ionic Conductivity. *Effect of Alkyl Chain Length.* Figure 5 shows the effect of alkylimidazolium chain length (alkyl = CH_3 (Me), *n*-C_4H_9 (Bu), or *n*-C_6H_{13} (Hex)) on the temperature-dependent in-plane ionic conductivity of the POIL diblock copolymer. All three polymers shown in Figure 5 have a similar morphology (lamellar), glass transition temperature of the POIL block (9 °C), POIL composition (15.6−17.0 mol %), and molecular weight (38.0−40.7 kg/mol) (Table 2). From these data it is clear that when all of these parameters are the same, the resulting ionic conductivities are similar.

Effect of Composition and Morphology. Figure 6 shows the temperature-dependent ionic conductivity of PS-*b*-PVBnHexImTFSI as a function of copolymer composition ranging from

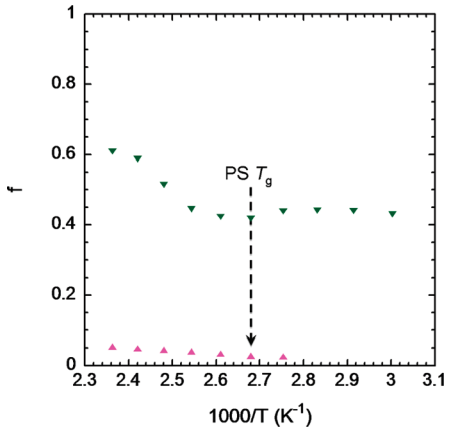

Figure 7. Plot of the normalized ionic conductivity or morphology factor f as a function of temperature for PS-*b*-PVBnHexImTFSI-17.0 (green ▼) and PS-*b*-PVBnHexImTFSI-8.6 (violet ▲) that emphasizes the effects of morphology and defects on block copolymer conductivity and highlights an increase in the conductivity of PS-*b*-PVBnHexImTFSI-17.0 near the glass transition temperature of poly(styrene).

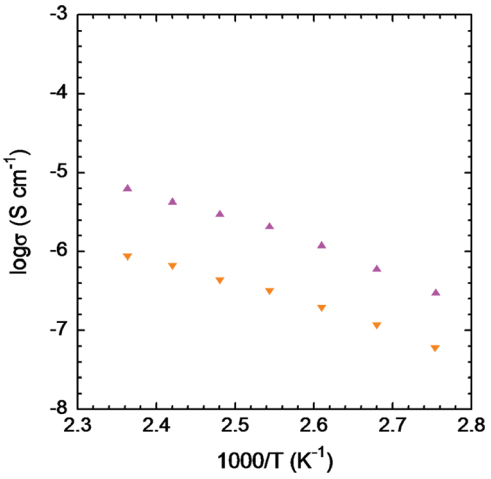

Figure 8. Temperature-dependent ionic conductivity for PS-*b*-PVBnHexImTFSI-8.6 films prepared by solvent-casting (violet ▲) and melt-pressing (orange ▼).

8.6 to 100 mol % POIL. Lower POIL block compositions (7.1 and 2.7 mol %) were too resistive to report accurate conductivity values. Since these samples exhibiting hexagonally packed cylindrical morphology have a low degree of long-range order, their poor in-plane ionic conductivity likely stems from numerous morphological defects and large numbers of grain boundaries that serve as "dead ends" for conductive channels (i.e., poor long-range ionic domain connectivity throughout the film). It is clear that the ionic conductivity increases significantly with increasing POIL block composition; however, it does so in a nonlinear fashion. Specifically, the in-plane conductivity increases by more than an order of magnitude when the POIL block composition is changed only 2-fold from 8.6 mol % POIL to 17.0 mol % POIL and increases approximately 5-fold when the POIL block composition is changed from 17.0 mol % POIL to 100 mol % POIL homopolymer. Since the nanoscale morphologies of the 8.6 mol % POIL and the 17.0 mol % POIL block copolymers are a coexistence of cylinders and lamellae (where the POIL block is the minor component) and pure lamellae, respectively, we speculate that the nonlinear relationship between ionic conductivity and POIL block composition must be due to morphological effects.

To account for the effects of morphology on ionic conductivity for a diblock copolymer that consists of one conducting component and one nonconducting component, Balsara and co-workers proposed a normalized ionic conductivity or a morphology factor, f:[23]

$$f = \frac{\sigma}{\phi_c \sigma_c} \quad (1)$$

where σ is the measured conductivity and φ_c and σ_c are the volume fraction and intrinsic conductivity of the conducting phase, respectively. Here, the ionic conductivity of homopolymer (PVBnHexImTFSI) was used as σ_c. Figure 7 compares the normalized conductivity for the block copolymer samples with a lamellar (17.0 mol %) and lamellar + cylindrical (8.6 mol %) morphology, corresponding to $\varphi_c = 0.50$ and 0.34, respectively (see Supporting Information for detailed volume fraction calculations). For the 17.0 mol % sample, the normalized in-plane conductivity ranges from 0.41 to 0.61, which is smaller than the predicted morphology factor, $f = {}^2/_3$, for randomly oriented lamellae,[23,37] suggesting that this sample has additional resistances that contribute to slightly less than ideal conductivities (e.g., grain boundaries). Figure 7 also shows that in the temperature range below 100 °C, the normalized conductivity is ~0.42. However, above 100 °C, the normalized conductivity increases from ~0.42 to ~0.61. Interestingly, 100 °C corresponds to the glass transition temperature of the styrene block, suggesting that the glass−liquid transition of the nonconducting microphase can impact ionic conductivity. A similar phenomenon was observed in previous work in ionic liquid-doped block copolymers.[25] For the 8.6 mol % sample, the normalized conductivity ranges from 0.03 to 0.05, which is an order of magnitude smaller than the predicted morphology factor, $f = {}^1/_3$, for randomly oriented conducting cylinders.[23,37] Since this sample exhibits coexistence between lamellae and cylinders, one would predict f to be an intermediate value between that expected for cylinders and lamellae ($^1/_3 < f < {}^2/_3$). This probably results from a lack of macroscopic connectivity of cylindrical microdomains across the film or other morphological defects that significantly limit ion conduction.

For the ionic conductivity data presented thus far, all of the polymer films were prepared by solvent casting. To examine the sole effect of morphology on ionic conductivity, the conductivity of the POIL diblock copolymer at a single POIL composition (8.6 mol %) was measured using two different film preparation techniques: solvent casting and melt pressing. Figure 8 shows the results, where the solvent-cast film, which exhibits good long-range order, has an in-plane conductivity approximately one order of magnitude higher than the more poorly ordered melt-pressed film. This result again exemplifies the importance of high degrees of connectivity among conducting domains, as morphological defects and grain boundaries serve as effective "dead ends" for ion conduction.

■ CONCLUSION

We synthesized a series of PS-*b*-PVBn(alkyl)ImTFSI diblock copolymers with varying compositions by post-polymerization functionalization of PS-*b*-PVBCl with homologous *N*-alkylimidazoles (alkyl = CH_3, *n*-C_4H_9, and *n*-C_6H_{13}). The block copolymers microphase separate into cylinders, lamellae, or coexistence of cylinders+lamellae with varying degrees of long-range order

depending on their composition and film-preparation technique (solvent-casting *vs* melt-pressing). Lamellar samples with similar compositions exhibited comparable values of conductivity (~0.1 mS cm^{-1} at 150 °C) regardless of imidazolium alkyl substituent. For a compositionally varied series of PS-*b*-PVBnHexImTFSI diblocks, conductivity was dependent on POIL composition, morphology, and degree of long-range order. For a lamellar sample (17.0 mol % POIL), conductivity was approximately 5-fold less than for the corresponding homopolymer. Moreover, in comparing a lamellar sample (17.0 mol %) to a lamellar + cylindrical coexistence sample (8.6 mol %), conductivity dropped off by more than an order of magnitude, indicating the potential for cylindrical domains to suffer from morphological defects and grain boundaries that decrease macroscopic connectivity and impede conductivity. Two films of a single sample (8.6 mol %) prepared by different techniques exemplified the importance of long-range order to achieve high conductivity, as the well-ordered solvent-cast film exhibited conductivities one order of magnitude greater than the poorly ordered melt-pressed film. Low POIL composition samples (2.7 and 7.1 mol % POIL) having poorly ordered cylindrical morphologies exhibited low conductivities below the measurement detection limit due to a large number of morphological defects (e.g., grain boundaries and "dead ends"). It is evident from this work that the conductivity of microphase separated ion conducting membranes are dependent on nanoscale morphology, specifically, the degree of connectivity of ionic domains. In particular, samples exhibiting a hexagonally packed cylinders morphology with a minority conducting phase ($\varphi_{POIL} < 0.5$) suffer from poor ionic conductivity due to their propensity for morphological defects and grain boundaries.

■ ASSOCIATED CONTENT

Supporting Information. Additional data including ^{1}H NMR spectrum of **1**, 2D SAXS patterns, variable-temperature SAXS profiles for all samples, an expansion of the SAXS profile for solvent-cast PS-*b*-PVBnHexImTFSI-8.6, and calculations of polymer volume fractions. This material is available free of charge via the Internet at http://pubs.acs.org/.

■ AUTHOR INFORMATION

Corresponding Author

*(M.K.M.) E-mail: mahesh@chem.wisc.edu. Telephone: +1 (608) 262-0421. (Y.A.E.) E-mail: elabd@drexel.edu. Telephone: +1 (215) 895-0986.

■ ACKNOWLEDGMENT

The authors gratefully acknowledge financial support from the University of Wisconsin-Madison, a National Science Foundation Graduate Research Fellowship to R.L.W., and U.S. Army Research Office under Grant W911NF-07-1 0452: Ionic Liquids in Electro-Active Devices (ILEAD) MURI. This research also made extensive use of UW-Madison MRSEC/NSEC characterization facilities (DMR-0520527 and DMR-0425880). SAXS data was acquired at the Advanced Photon Source DuPont-Northwestern-Dow Collaborative Access Team beamline (Sector 5), which is supported by E. I. DuPont de Nemours & Co., the Dow Chemical Company, the State of Illinois, and the U.S. Department of Energy, Office of Basic Energy Sciences (Contract No. DE-AC02-06CH11357).

■ REFERENCES

(1) Kim, J.-H.; Kim, J.-W.; Shokouhimehr, M.; Lee, Y.-S. *J. Org. Chem.* **2005**, *70*, 6714.
(2) Yang, X.; Fei, Z.; Zhao, D.; Ang, W. H.; Li, Y.; Dyson, P. J. *Inorg. Chem.* **2008**, *47*, 3292.
(3) Yuan, J. Y.; Giordano, C.; Antonietti, M. *Chem. Mater.* **2010**, *22*, 5003.
(4) Bara, J. E.; Camper, D. E.; Gin, D. L.; Noble, R. D. *Acc. Chem. Res.* **2010**, *43*, 152.
(5) Bara, J. E.; Noble, R. D.; Gin, D. L. *Ind. Eng. Chem. Res.* **2009**, *48*, 4607.
(6) Tang, J. B.; Shen, Y. Q.; Radosz, M.; Sun, W. L. *Ind. Eng. Chem. Res.* **2009**, *48*, 9113.
(7) Tang, J.; Tang, H.; Sun, W.; Plancher, H.; Radosz, M.; Shen, Y. *Chem. Commun.* **2005**, 3325.
(8) Green, O.; Grubjesic, S.; Lee, S.; Firestone, M. *Polym. Rev.* **2009**, *49*, 339.
(9) Armand, M.; Endres, F.; MacFarlane, D. R.; Ohno, H.; Scrosati, B. *Nat. Mater.* **2009**, *8*, 621.
(10) Lodge, T. P. *Science* **2008**, *321*, 50.
(11) Gu, Y.; Lodge, T. P. *Macromolecules* **2011**, *44*, 1732.
(12) Zhang, S.; Lee, K. H.; Frisbie, C. D.; Lodge, T. P. *Macromolecules* **2011**, *44*, 940.
(13) Yoshizawa, M.; Ohno, H. *Electrochim. Acta* **2001**, *46*, 1723.
(14) Chen, H.; Choi, J.-H.; Salas-de la Cruz, D.; Winey, K. I.; Elabd, Y. A. *Macromolecules* **2009**, *42*, 4809.
(15) Ye, Y.; Elabd, Y. A. *Polymer* **2011**, *52*, 1309.
(16) Clark, T. J.; Robertson, N. J.; Kostalik, H. A.; Lobkovsky, E. B.; Mutolo, P. F.; Abruña, H. D.; Coates, G. W. *J. Am. Chem. Soc.* **2009**, *131*, 12888.
(17) Robertson, N. J.; Kostalik, H. A.; Clark, T. J.; Mutolo, P. F.; Abruña, H. D.; Coates, G. W. *J. Am. Chem. Soc.* **2010**, *132*, 3400.
(18) Varcoe, J. R.; Slade, R. C. T.; Lam How Yee, E. *Chem. Commun.* **2006**, 1428.
(19) Sun, X. G.; Kerr, J. B. *Macromolecules* **2006**, *39*, 362.
(20) Matsumoto, K.; Endo, T. *Macromolecules* **2009**, *42*, 4580.
(21) Matsumoto, K.; Endo, T. *J. Polym. Sci., Part A: Polym. Chem.* **2010**, *48*, 3113.
(22) Elabd, Y. A.; Hickner, M. A. *Macromolecules* **2011**, *44*, 1.
(23) Wanakule, N. S.; Panday, A.; Mullin, S. A.; Gann, E.; Hexemer, A.; Balsara, N. P. *Macromolecules* **2009**, *42*, 5642.
(24) Simone, P. M.; Lodge, T. P. *ACS Appl. Mater. Interfaces* **2009**, *1*, 2812.
(25) Gwee, L.; Choi, J.-H.; Winey, K. I.; Elabd, Y. A. *Polymer* **2010**.
(26) Lee, M.; Choi, U. H.; Colby, R. H.; Gibson, H. W. *Chem. Mater.* **2010**, *22*, 5814.
(27) Hoshino, K.; Yoshio, M.; Mukai, T.; Kishimoto, K.; Ohno, H.; Kato, T. *J. Polym. Sci., Part A: Polym. Chem.* **2003**, *41*, 3486.
(28) Weber, R. L.; Ye, Y.; Banik, S. M.; Elabd, Y. A.; Hickner, M. A.; Mahanthappa, M. K. Submitted for publication.
(29) Armarego, W. L. F.; Chai, C. L. L. *Purification of laboratory chemicals*, 5th ed.; Butterworth-Heinemann: Amsterdam and Boston, MA, 2003.
(30) Pernak, J.; Feder-Kubis, J.; Cieniecka-Roslonkiewicz, A.; Fischmeister, C.; Griffin, S. T.; Rogers, R. D. *New J. Chem.* **2007**, *31*, 879.
(31) Benoit, D.; Chaplinski, V.; Braslau, R.; Hawker, C. J. *J. Am. Chem. Soc.* **1999**, *121*, 3904.
(32) Alyea, H. N. *J. Chem. Educ.* **1971**, *48*, 389.
(33) Stancik, C. M.; Lavoie, A. R.; Schütz, J.; Achurra, P. A.; Lindner, P.; Gast, A. P.; Waymouth, R. M. *Langmuir* **2004**, *20*, 596.
(34) Park, M. J.; Balsara, N. P. *Macromolecules* **2010**, *43*, 292.
(35) Roe, R. J. *Methods of X-ray and neutron scattering in polymer science*; Oxford University Press: New York, 2000.
(36) Lynd, N. A.; Hillmyer, M. A. *Macromolecules* **2005**, *38*, 8803.
(37) Sax, J.; Ottino, J. M. *Polym. Eng. Sci.* **1983**, *23*, 165.